



New tracking modes and performance for Mars spacecraft orbit determination and lander positioning



Jianguo Yan^a, Xuan Yang^a, Mao Ye^{a,f,*}, Fei Li^a, Shuanggen Jin^{b,c}, Weitong Jin^a, Jean-Pierre Barriot^{a,d}, Haitao Li^e

^a State Key Laboratory of Information Engineering in Surveying, Mapping and Remote Sensing, Wuhan University, Wuhan 430070, China

^b Shanghai Astronomical Observatory, Chinese Academy of Science, Shanghai 200030, China

^c Department of Geomatics Engineering, Bulent Ecevit University, Zonguldak 67100, Turkey

^d Observatoire géodésique de Tahiti, Tahiti 98702, French Polynesia

^e Beijing Institute of Tracking and Telecommunications Technology, Beijing 100094, China

^f CAS Key Laboratory of Planetary Sciences, Shanghai, 200030, China

ARTICLE INFO

Keywords:

POD

Lander positioning

Same-beam differential VLBI

Three-way loop Doppler

ABSTRACT

Precise orbit determination and lander positioning are still a challenge for Mars exploration. In this paper, three positioning methods are proposed, including the same-beam differential Very Long Baseline Interferometry (VLBI), four-way orbiter-lander Doppler and three-way loop Doppler for Mars orbiter and lander. Measurement models and these three positioning methods are further analyzed and evaluated using simulation experiments. The results show that about 60-m level accuracy for the Mars lander can be achieved by a combination same-beam differential VLBI data at 10 ps noise level with two-way Doppler data at the 0.1 mm/s noise level. Since VLBI data are sensitive to the angle between two radio sources, the accuracy of the Mars orbiter was not improved. The geometry of four-way orbiter-lander Doppler is more sensitive than the geometry of ordinary two-way Doppler, and therefore, after adding the four-way orbiter-lander Doppler data, the accuracy of the orbiter and lander positioning can reach the meter and decimeter level. Furthermore, the three-way loop Doppler reduces the number of orbital repeater signals and improves the POD accuracy at the meter level as well as the lander positioning accuracy at the decimeter level. Therefore, the three-way loop tracking mode provides an important reference for future Mars missions.

1. Introduction

Different types of detectors in deep-space missions can obtain comprehensive and precise scientific data in orbiting, landing, and sampling tasks (Liu et al., 2015; Jin et al., 2013; Wei et al., 2013; Jin and Zhang, 2014; Tenzer et al., 2015a; 2015b). Multi-mode detection in deep space often requires various detectors work together; therefore, the first problem to solve is multi-detector simultaneous positioning (Liu et al., 2017, 2018).

In the Selenological and Engineering Explorer (SELENE) mission, the same-beam differential VLBI was successfully implemented on the Rstar and Vstar sub-satellites (Namiki et al., 1999). The orbital accuracy reached at 10 m, and improved the accuracy of the low-order gravity field model of the moon (Goossens et al., 2009; Liu et al., 2010). In addition, the same-beam differential VLBI was complimented using two

detectors focused on the moon, Venus, or Mars in the past (Counselman et al., 1972; King et al., 1976; Smith and Ramos, 1980; Preston et al., 1986; Edwards et al., 1991; Kahn et al., 1992; Border et al., 1991; Nandi et al., 1993). The same-beam differential VLBI provides plane-of-sky relative position change information at high accuracy. Also, the same-beam differential VLBI eliminates or reduces most of the systematic errors in observations stemming from the ionosphere, and troposphere interference as well noise from the receiver during the correlation phase. A joint solution for the positioning of orbiter and lander, theoretically, will provide better accuracy for three-dimensional positioning than solutions using only Doppler data that is only sensitive in the line-of-sight direction.

In addition, Four-way Doppler was implemented for the first time during the SELENE mission on a near circular lunar satellite and a high-eccentric relay orbiter. Earth tracking stations cannot track satellites on

* Corresponding author.

E-mail address: mye@whu.edu.cn (M. Ye).

the far side of the moon directly. The successful implementation of this technology solved that problem allowing the collection of information about the lunar gravity field on the far side. Hence, this technology had improved the accuracy of the lunar gravity field model (Namiki et al., 2009; Hanada et al., 2008; Matsumoto et al., 2008).

However, it is still challenging to get precise orbit determination and lander positioning for Mars exploration currently. Multi-technique joint positioning is significant to improve the success of Mars missions. In this paper, three new methods, same-beam differential VLBI, four-way orbiter-lander Doppler, and three-way loop Doppler, are proposed for orbiter determination and lander positioning based on the multi-detector model. The paper is organized as follows: Section 2 describes the measurement model for same-beam differential VLBI, the four-way orbiter-lander Doppler model, and the three-way loop Doppler. Section 3 shows simulation results and discussions, and finally conclusions and perspectives are given in Section 4.

2. Methods and models

2.1. Same-beam differential VLBI model

The Same-beam differential VLBI is implemented as follows: the signals from two spacecraft are received at the same time on the same beam width by two Earth-based antennas. The observations are based on the delay between the arrival times of a radio source at two different stations constituting a baseline, and carries information on the angular position of the source (Thornton and Border, 2000; Goossens et al., 2011). The principle of the same-beam differential VLBI observation equations are shown in Fig. 1. T_1 and T_2 are the Earth-based tracking stations and $\tau_{T_1}^{S_m}$ represents the light travel time of the signal from the Mars orbiter to the Earth station T_1 . Similarly, $\tau_{T_1}^{L_k}$ and $\tau_{T_2}^{L_k}$ denote the signals round-trip light time from Mars lander to the Earth stations T_1 and T_2 , respectively.

Aligning the signal phase to the same wave front makes it possible to obtain accurate same-beam differential VLBI data (Chen and Liu, 2010). The measurement model of same-beam differential VLBI aligned to the same wave front differential phase delays can be expressed as:

$$\tau = \tau^{S_m} - \tau^{L_k} = (\tau_{T_2}^{S_m} - \tau_{T_1}^{S_m}) - (\tau_{T_2}^{L_k} - \tau_{T_1}^{L_k}) \quad (1)$$

Further, τ^{S_m} and τ^{L_k} could be shown as:

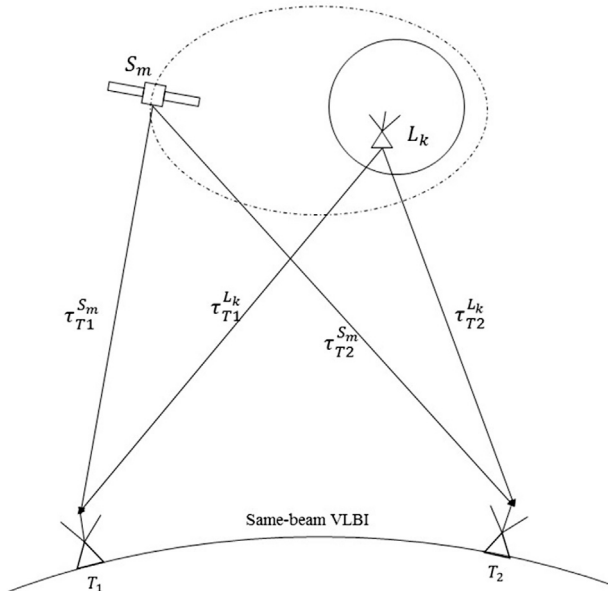


Fig. 1. Schematic diagram of same-beam differential VLBI model.

$$\tau^{S_m} = \frac{r_{S_2} - r_{S_1}}{c} + (RLT_{S_2} - RLT_{S_1}) + \{[t_1(TDB) - t_1(UTC)] - [t_2(TDB) - t_2(UTC)]\} \quad (2)$$

$$\tau^{L_k} = \frac{r_{L_2} - r_{L_1}}{c} + (RLT_{L_2} - RLT_{L_1}) + \{[t_1(TDB) - t_1(UTC)] - [t_2'(TDB) - t_2'(UTC)]\} \quad (3)$$

$$r_{S_2} = |X(S_m) - X(T_2)| \quad (4)$$

$$r_{S_1} = |X(S_m) - X(T_1)| \quad (5)$$

$$r_{L_2} = |X(L_k) - X(T_2')| \quad (6)$$

$$r_{L_1} = |X(L_k) - X(T_1)| \quad (7)$$

where $X(S_m)$ represents the position state of the orbiter at time m , $X(T_1)$ is the position vector of tracking station T_1 on the Earth, $X(L_k)$ is the position vector of the lander L_k at time k , $X(T_2)$ and $X(T_2')$ indicates different position vectors of station T_2 because the former is the time received from the orbiter. The latter value is the time a signal received from the lander. In the implementation of same-beam differential VLBI, T_1 is the main station and the time scale of the observations is $t_1(UTC)$. Since the positions of the two spacecrafts are different, the time of t_2 and t_2' in equation (2) and in equation (3) are different. The values r_{S_1} and r_{S_2} represent the geometric distance of the signal transmitted from the orbiter to the station T_1 and T_2 . The values r_{L_1} and r_{L_2} represent the geometric distance of the signal transmitted from the Mars Lander to the Earth station T_1 and T_2 , respectively; RLT_{S_2} and RLT_{S_1} are the relativistic time delays for the orbiter to station T_2 and T_1 , called the Shapiro delay (Shapiro, 1964; Moyer, 2005; Tommei et al., 2010). The values RLT_{L_2} and RLT_{L_1} are Shapiro delay for the Mars Lander to station T_2 and T_1 . As observations recorded by deep space network (DSN) stations are given in UTC time, corresponding time-scale corrections are required. The third and fourth terms in equations (2) and (3) represent the time-scale corrections converting UTC to TDB.

From equation (1), the partial derivatives of the same-beam differential VLBI observations to the Mars orbiter are obtained as:

$$\frac{\partial \tau}{\partial x_{S_m}} = \left(\frac{X(S_m) - X(T_2)}{|X(S_m) - X(T_2)|} - \frac{X(S_m) - X(T_1)}{|X(S_m) - X(T_1)|} \right) \cdot \frac{1}{c} \quad (8)$$

Moreover, the partial derivative to the Mars Lander is:

$$\frac{\partial \tau}{\partial x_{L_k}} = - \left(\frac{X(L_k) - X(T_2')}{|X(L_k) - X(T_2')|} - \frac{X(L_k) - X(T_1)}{|X(L_k) - X(T_1)|} \right) \cdot \frac{1}{c} \quad (9)$$

2.2. The four-way Doppler model

We extended the four-way Doppler model to Mars Mission. The key technology in four-way orbiter-lander Doppler enables signal relays by satellite. The concept is shown in Fig. 2. The Earth tracking station sends an uplink frequency to the orbiter at epoch T_i , then the orbiter receives the signal at epoch S_j and immediately relays to the lander, and the lander receives and relays the signal at epoch L_k to the orbiter. The signal is re-transmitted back the Earth at epoch S_m and tracking station on the Earth will ultimately receive the downlink signal at epoch T_n .

The computation of the range rate measurement for the four-way orbiter-lander Doppler is similar to the traditional two-way Doppler. The backtracking method is applied according to the path of T_n - S_m - L_k - S_j - T_i , followed by time forward projections (Moyer, 2005). The Earth station receives downlink signal at time T_n and records the time tag. However, the rest of the time (S_m - L_k - S_j - T_i) are unknown. The downlink signal arrival times (T_n) are given in Coordinated Universal Time (UTC) written as UTC (T_n). At first, T_n must be converted into the

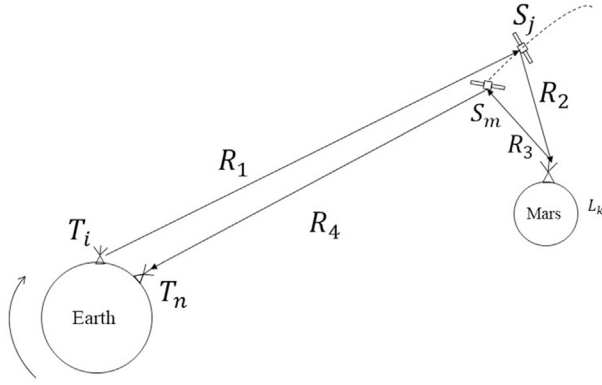


Fig. 2. Schematic diagram of four-way Doppler model.

TDB time scale, TDB (T_n). Then TDB (S_m), TDB (L_k), TDB (S_j) and TDB (T_i) can be obtained by the light-time solution (Moyer, 2005), and finally TDB (T_i) is converted to UTC time, UTC (T_i). The whole calculation process is carried out in the Barycentric Celestial Reference System (BCRS). The range-rate measurement model can be expressed as:

$$R = (R_1 + c \cdot RL T_{nm}) + R_2 + R_3 + (R_4 + c \cdot RL T_{ij}) + c \cdot [TDB(T_i) - UTC(T_i)] - c \cdot [TDB(T_n) - UTC(T_n)] = c \cdot [UTC(T_n) - UTC(T_i)] \quad (10)$$

$$R_1 = |X(S_m) - X(T_n)| \quad (11)$$

$$R_2 = |X(S_m) - X(L_k)| \quad (12)$$

$$R_3 = |X(S_j) - X(L_k)| \quad (13)$$

$$R_4 = |X(S_j) - X(T_i)| \quad (14)$$

where R_1 , R_2 , R_3 , and R_4 represent the geometric distance as shown in Fig. 2, $X(S_m)$, $X(S_j)$, $X(T_i)$, $X(T_n)$, and $X(L_k)$ represent the position vector expressed in BCRS. Since the distance from Mars orbiter to the lander is relatively small, the relativistic delay between the lander and the orbiter is not considered in equation (10). The calculation of the range rate measurement is expressed in the integral Doppler form. In one Doppler integration period, the range rate measurement can be described as the rate of the distance change between the start time T_s and the end time T_e . R_s and R_e are obtained by equation (10) at epochs T_s and T_e . The range rate can be expressed as:

$$\dot{R} = \frac{(R_e - R_s)}{T_e - T_s} \quad (15)$$

For the calculation of the partial derivative, according to equation (10), we can deduce the partial derivative of the distance to the orbiter and the lander as:

$$\frac{\partial R}{\partial S_j} = \frac{X(S_j) - X(T_i)}{|X(S_j) - X(T_i)|} + \frac{X(S_j) - X(L_k)}{|X(S_j) - X(L_k)|} \quad (16)$$

$$\frac{\partial R}{\partial S_m} = \frac{X(S_m) - X(T_n)}{|X(S_m) - X(T_n)|} + \frac{X(S_m) - X(L_k)}{|X(S_m) - X(L_k)|} \quad (17)$$

$$\frac{\partial R}{\partial L_k} = \frac{X(L_k) - X(S_j)}{|X(L_k) - X(S_j)|} + \frac{X(L_k) - X(S_m)}{|X(L_k) - X(S_m)|} \quad (18)$$

2.3. Three-way loop measurement model

A new measurement model, named three-way loop Doppler based on the four-way orbiter-lander Doppler model is proposed. The difference between this new model and four-way orbiter-lander Doppler is that three-way loop measurement reduces the number of links between the Mars lander and the orbiter and instead, transmits a downlink signal directly from Mars lander to an Earth tracking station. The schematic diagram of three-way loop Doppler measurement model is shown in Fig. 3. The Earth tracking station sends an uplink frequency to the Mars orbiter at epoch T_i , and the signal is received at the Mars orbiter at epoch S_j ; the Mars Lander at epoch L_k receives the signal from the orbiter. The signal is re-transmitted back the Earth by the transponder on the orbiter and received by tracking station at epoch T_n .

Similar to the four-way orbiter-lander model, the three-way loop model also uses “backtracking” to calculate the range, based on the $T_n - L_k - S_j - T_i$ path. This distance model can be expressed as:

$$R = (R_1 + c \cdot RL T_{nk}) + R_2 + (R_3 + c \cdot RL T_{ij}) + c \cdot [TDB(T_i) - UTC(T_i)] - c \cdot [TDB(T_n) - UTC(T_n)] = c \cdot [UTC(T_n) - UTC(T_i)] \quad (19)$$

$$R_1 = |X(S_j) - X(T_i)| \quad (20)$$

$$R_2 = |X(S_j) - X(L_k)| \quad (21)$$

$$R_3 = |X(T_n) - X(L_k)| \quad (22)$$

Similarly, the range rate model can be expressed by equation (15).

The partial derivative is calculated as follows:

$$\frac{\partial R}{\partial S_j} = \frac{X(S_j) - X(T_i)}{|X(S_j) - X(T_i)|} + \frac{X(S_j) - X(L_k)}{|X(S_j) - X(L_k)|} \quad (23)$$

$$\frac{\partial R}{\partial L_k} = \frac{X(L_k) - X(S_j)}{|X(L_k) - X(S_j)|} + \frac{X(L_k) - X(T_n)}{|X(L_k) - X(T_n)|} \quad (24)$$

The three-way loop Doppler mode has reduced a link and therefore is reliable and relatively simple to implement, unlike the four-way orbiter-lander Doppler mode. Meanwhile, by adding a link between the orbiter and the lander, and a link between the lander and the Earth tracking station, the three-way orbiter-lander Doppler mode can resolve the position of orbiter and the lander at the same time, unlike the two-way Doppler mode. Given the massively increasing volume of tracking data, we think that three-way loop Doppler mode is the optimum solution for solving Orientation and rotation Parameters of Mars.

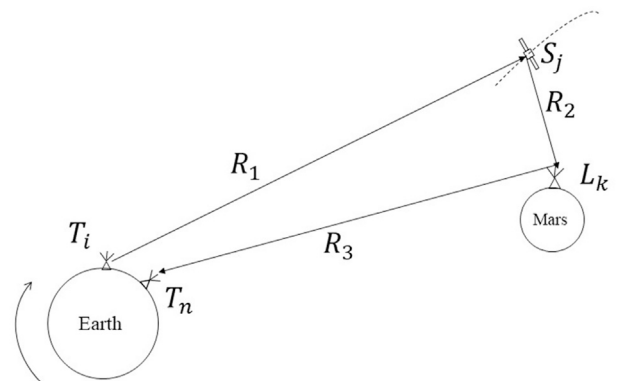


Fig. 3. Schematic diagram of three-way loop measurement model.

3. Simulation results and analysis

We independently developed the Mars Gravity Recovery and Analysis Software (MAGREAS), which is part of Wuhan University Deep Space Orbit determination and Gravity Recovery System software (Ye, 2016; Yan et al., 2017; Yan et al., 2017) in order to enhance the capability of Mars spacecraft precise orbit determination and recover the Martian gravity field model. Our simulation was based on the MAGREAS. During the simulation, we applied three new Mars measurement models as described in section 2, and evaluated the accuracy of Mars Lander positioning and the orbit determination for the orbiter. The contributions of the three new tracking modes are investigated for the positioning of the Mars spacecraft relative to the traditional two-way tracking mode.

In Table 1, we present a typical Mars spacecraft orbit in this simulation with choosing an attractive lander site located in the Amazonis Planitia (30°N, 165°W), due to its low altitude, flatness, potential water history signature and its location near Olympus Mons. Fig. 4 shows the Martian topography and our chosen landing site. The map source data came from NASA, collected by the Mars orbiter laser altimeter (MOLA) science team (Smith et al., 2001a,b).

The Chinese Lunar Exploration Program (CLEP) is developing rapidly with subsequently more Chinese Deep Space Network (CDSN) (Dong et al., 2016). Now the CDSN consists of three globally distributed Chinese Deep Space Stations (CDSSs), including the Jiamusi station (66 m dish), the Kashi station (35 m dish) and the Zapala station (35 m antenna) in Neuquén, Argentina. These sites provide near continuous tracking of interplanetary spacecraft, as the Earth rotates.

The data processing method is based on the classical dynamical orbit determination theory (Montenbruck and Eberhard, 2012; Tapley et al., 2004). The local parameters include six initial orbital elements while the Lander position can be treated as a global parameter. After precise orbit determination for each arc, local parameters can be solved, and then, normal matrices obtained from each arc solution. The global parameters can be obtained by integrating the multi-arc normal matrices. The global iterations do not stop until the results of the global parameters converge. The algorithm process is similar to gravity field recovery (Yan et al., 2012).

3.1. Simulation and analysis of same-beam differential VLBI

The simulation strategy is shown in Table 2. Based on the dynamic models from Table 2, the true orbit was generated by integrating the motion equation with the initial orbit elements, and the orbits were then used to create simulated two-way data and same-beam differential VLBI data. The Earth stations for simulated two-way Doppler data are Jiamusi, Kash, and Zapala stations. Gaussian white noise with 1 sigma value of 0.1 mm/s and 10 ps were added to the two-way Doppler data and same-beam differential VLBI data. If the influence of the Mars atmosphere and ionosphere is not taken into account (Jin et al., 2004, 2016), there would be bias in the same-beam VLBI observables; hence, we added a measurement bias of 20 ps in these simulated observables. The sampling rate was 5 s. The tracking stations for same-beam differential VLBI were China VLBI Network (CVN), located in Seshan, Beijing, Kunming, and Urumqi. The arc length was one Earth day. Perturbations considered in the simulation included non-spherical gravitational perturbation, N-body perturbations, solar pressure, Phobos and Deimos perturbations, Martian atmospheric friction, relativistic effects, and the Martian solid tide.

In order to make the simulation more convincing, we added

Table 1
The orbital elements used in the simulation.

Semi major axis (m)	Eccentricity	Inclination (degree)	RAAN (degree)	argument of perigee (degree)	mean anomaly (degree)
7617819.000	0.495	15.666	119.478	323.181	87.152

systematic errors in the observables of the lander and orbiter, including a Lander position error of 1 km in each of the X-Y-Z components and deviation of 100 m at the initial orbit elements. Further, errors were added at factor of three to the uncertainty in the gravity field coefficient. Table 3 shows the simulation results of orbit determination and Table 4 shows the results of lander positioning.

We can see that after we included the same-beam differential VLBI data, the accuracy of the orbit have no significant improvement when compared to the results from only two-way Doppler. However, it can be used to solve the Lander's position. Table 4 shows that gravity field model errors and measurement bias degrade lander positioning accuracy a little (Wei et al., 2016), but have no influence on the error bar. The convergence speed was fast and took only three iterations. The positioning accuracy of the lander was about 32 m at the 10ps noise level. In addition, we also simulated the influence of different levels of noise in the same-beam differential VLBI data for the lander positioning accuracy. Taking into account that gravity field error may obscure the ability of same-beam differential VLBI positioning, we ignored gravity field error so that the results directly reveal how accurate the proposed method might be for lander positioning; these results are given in Table 5.

As seen in Table 5, the positioning accuracy of the lander could be increased by one order of magnitude for each order of magnitude improvement in same-beam differential VLBI data, when potential errors in coordinate transformation and other model errors are ignored. In general, this simulation of same-beam differential VLBI indicates that the proposed method can deliver precise Mars lander positions, while making a complimentary contribution to precise orbit determination when combined with two-way Doppler data.

3.2. Simulation and analysis of four-way orbiter-lander Doppler

In this simulation, the parameters and dynamic models are as those discussed in section 3.1. The Kash and Zapala stations transmit and receive two-way Doppler frequencies, and the tracking station in Jiamusi receives and transmits four-way orbiter-lander Doppler signals. Gaussian white noise with sigma of 0.1 mm/s was added to the two-way Doppler observables. Taking into account data transmission with low code rate and data loss, one sigma of 1 mm/s noise was added to the four-way Doppler observables. In addition to systematic errors and gravity field model errors in the lander and orbiter data, pass-dependent measurement biases at 2 mm/s were considered in four-way Doppler observables.

Four-way orbiter-lander Doppler data depends on the geometry between the earth tracking station, Mars orbiter and lander. In Table 6, we show a comparison of the number of the four-way orbiter-lander Doppler data and two-way Doppler data. The distribution of the tracking data is shown in Fig. 5.

From Table 6 and Fig. 5, the number of four-way Doppler data was influenced by occultation of the Earth and Mars. The premise when implementing four-way Doppler is that the orbiter and the Earth tracking station can see each other, and the orbiter and the lander are visible to each other as well. Overall, four-way Doppler data accounted for about 15% of the two-way Doppler data. In addition, we found that the observation conditions at the Zapala station were better than other two tracking stations, as the Zapala station has a maximum altitude of 65°. This station will improve the tracking capabilities of the deep space network in China.

In Table 7, we show the results of the Mars orbiter precise orbit determination using the two-way Doppler data and four-way orbiter-lander Doppler data. In Table 8, we list the computing process for lander positioning using the four-way orbiter-lander Doppler data.

The accuracy of some of the arc solutions improves a factor of two after adding the four-way Doppler data (arc No. 3, arc No. 5, and arc No. 6), but there are some arcs whose accuracy is decreased a little (arc No. 1, arc No. 2, arc No. 4 and arc No. 7). The reason is that these arcs accuracy (arc No. 1, arc No. 2, and arc No. 4 and arc No. 7) are precise enough before combining four-way Doppler data, so four-way data at 1 mm/s

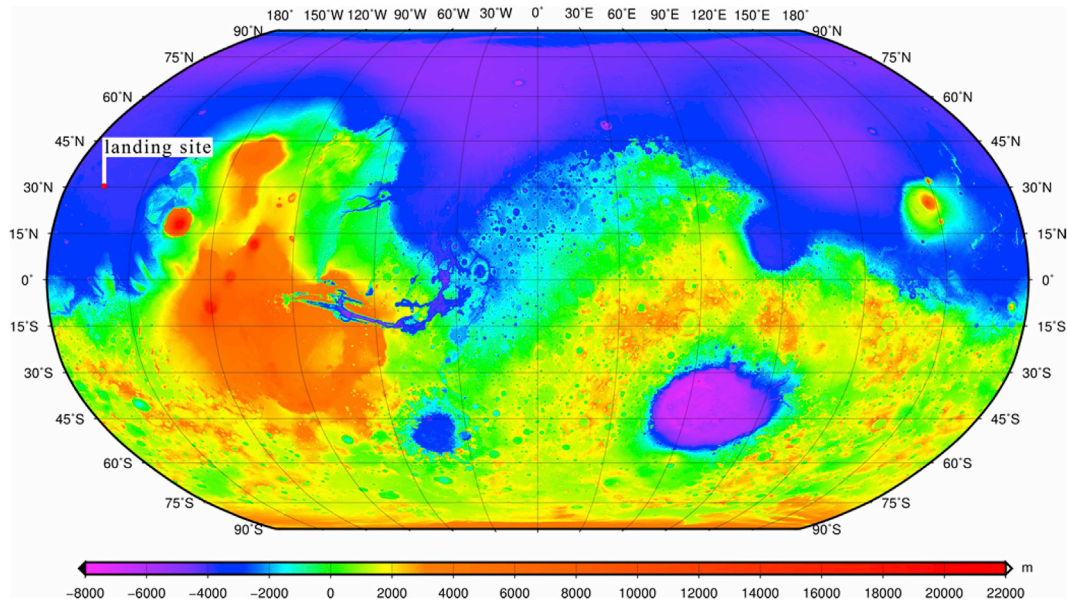


Fig. 4. Mars lander sites distribution.

Table 2
Simulation strategy in WUDOGS.

	Description
Arc length	24 h
The Orbiter	Large eccentricity and elliptical orbit with 450×8000 km height
The Mars lander	Location ($30^{\circ}00'00''$, $-160^{\circ}00'00''$) Cutoff angle 5°
Earth tracking station	Solid earth tide displacement $H2 = 0.6078$, $L2 = 0.0847$ Cutoff angle 5°
Dynamic models for the Orbiter	Non-spherical perturbation, MRO120D (Konopliv et al., 2016) Three body perturbation, DE421 used (Williams et al., 2008), including Phobos and Deimos perturbation K2 tidal perturbation, $K2 = 0.169$ Solar pressure perturbation Martian atmospheric drag (Stewart, 1987) Relativistic point mass acceleration and geodetic precession (Huang et al., 1990)

noise level may contaminate the result of high-precision accuracy to some extent, but the influence is limited.

In Table 8, we present the Mars lander positioning results, including two cases: one without added gravity field model error and measurement bias and the other with considering these sources of errors. The two cases both reached the decimeter level after convergence. Thus, the uncertainty in the gravity field model and the measurement bias had little influence on the lander positioning for the four-way Doppler observables.

In order to present the improvement in orbit accuracy after using

Table 3

Initial orbit position difference between solution and true one using the same-beam differential VLBI and two-way Doppler data in Mars J2000 system (estimated bias values, with the Landers position error of 100 m deviation and gravity error with a factor of three of the gravity field coefficient uncertainty). The errors denote the absolute difference from the true value.

Arc No.	Two-way Doppler only				Two-way Doppler with Same-beam differential VLBI of 10 ps noise				Bias (ps)
	Δx (m)	Δy (m)	Δz (m)	Errors(m)	Δx (m)	Δy (m)	Δz (m)	Errors(m)	
1	2.342	-3.450	-1.861	4.566	2.076	-3.059	-1.667	4.055	19.999
2	0.268	-0.115	-0.761	0.815	0.872	-0.433	-2.671	2.843	20.001
3	0.313	0.741	-3.030	3.135	0.293	0.690	-2.852	2.948	20.000
4	0.106	-0.186	0.380	0.436	0.117	-0.355	0.649	0.748	19.999
5	1.551	1.371	-2.689	3.393	1.586	1.414	-2.787	3.504	20.000
6	1.789	0.176	-7.484	7.697	1.981	0.194	-8.287	8.522	19.999
7	-0.081	0.172	-0.076	0.204	-0.296	0.587	-0.301	0.723	19.999

four-way data, we present the orbital differences of two arcs with considering gravity field model error and measurement bias in Fig. 6. This figure shows the orbit differences between the true orbit and the reconstructed orbit constructed from the two-way data only (left row), and the orbit differences from the two-way and four-way data together (right row). Differences are given in three components (R, radial; T, tangential and N, normal).

These results reveal that the differences in directions T and N are reduced doubly after the four-way Doppler data are included. Thus, four-way data improved orbit accuracy to some extent. In this simulation, we ignored the effect of the Mars atmosphere and ionosphere on the four-way Doppler link. These errors could be reduced during data pre-processing and estimated into the systematic measurement bias.

3.3. Simulation and analysis of three-way loop Doppler

Taking into account that the three-way loop Doppler model is similar to four-way orbiter-lander Doppler, we set the three-way loop Doppler to a similar configuration as those discussed in section 3.2, and shown in Table 2. Gaussian white noise with one sigma of 0.1 mm/s was added to the two-way Doppler observables. One sigma of 1 mm/s Gaussian noise and measurement bias of 2 mm/s were added to the three-way loop Doppler observables. In the three-way loop Doppler model, the signal is directly transmitted to Earth after the lander receives the signal from the orbiter. The simulated data include two-way Doppler and three-way loop Doppler. The deep space tracking station in Jiamusi transmits and receives three-way loop Doppler signals; the Kashi and Zapala stations transmit and receive two-way Doppler signals. The sampling rate was set

Table 4

The iterative process for the lander position using the same-beam differential VLBI data with 10 ps noise. The errors denote the absolute difference with the true value, and triple standard deviation is used to represent the uncertainty of the results.

Number of iterations	without the gravity field model errors and measurement bias			with the gravity field model errors and measurement bias		
	Δx (m)	Δy (m)	Δz (m)	Δx (m)	Δy (m)	Δz (m)
1	-1003.005	-974.060	994.485	-1008.613	-980.512	993.310
2	-9.487	-3.787	-0.386	-15.031	2.409	-0.314
3	-0.194	-0.148	-0.074	0.214	-0.837	0.867
Total	-1012.686	-977.995	994.025	-1023.430	-978.940	993.863
Errors	12.686	-23.005	5.975	23.430	-21.060	7.137
3 σ	± 32.661	± 20.812	± 59.075	± 32.661	± 20.811	± 59.075

Table 5

The positioning accuracy of lander using different noise of same-beam differential VLBI data (without the gravity field model errors).

Random noise		0.1 ns	10 ps	1 ps
Position errors	$\Delta X(m)$	129.242 \pm 133.882	12.686 \pm 32.661	-1.154 \pm 2.556
	$\Delta Y(m)$	237.947 \pm 212.773	-23.005 \pm 20.812	6.8433 \pm .678
	$\Delta Z(m)$	-24.555 \pm 116.547	5.975 \pm 59.075	-0.484 \pm 4.366

Table 6

The number of four-way Doppler data and two-way Doppler data.

Arc No.	Kashi	Jiamusi	Agrio
	2WRR	4WRR	2WRR
1	3272	668	4188
2	3262	1760	4197
3	3252	844	4207
4	3240	597	4216
5	3231	2053	4225
6	3220	1367	4235
7	3210	450	4243

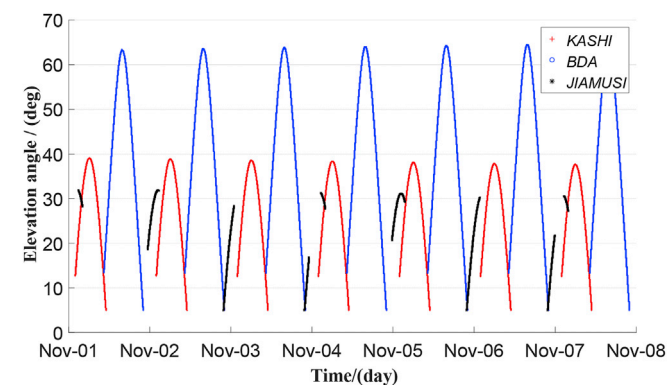


Fig. 5. The distribution of Four-way Doppler data and two-way Doppler data (The vertical axis is the elevation angle observed by the station, and the horizontal axis is the time).

to 5 s. The precision orbit determination and lander positioning results are given in Tables 9 and 10.

In Table 9, the combination of the three-way loop Doppler and two-way Doppler resulted in limited improvement to the orbital accuracy as compared with the solution from two-way Doppler data alone. This is because the noise level of three-way close loop Doppler data is at 1 mm/s, which is an order of magnitude bigger than the two-way Doppler data. However, the orbital accuracy of arc No.3, arc No.5, and arc No.6 improved slightly. The accuracy of lander positioning reaches the decimeter level, which is better than the positioning results from the same-beam differential VLBI model. In order to investigate the merit of this three-way loop Doppler, another experiment, considering that the observables are always affected by the orbital errors, was executed, testing

the influence of orbital errors on lander positioning. Ten meter errors in each X-Y-Z components of orbit were added and not adjusted; these lander-positioning results are shown in Table 11.

Three-way loop Doppler model has better accuracy than the four-way Doppler model shown in Table 11. The reason is that the former model has a direct link to the Earth tracking station, which provides a constraint on lander positioning. The latter model however, only links with the orbiter so that the orbital errors have more influence on lander positioning.

3.4. Discussion

In order to show the contribution of these methods in orbit determination clearly, the initial orbit position difference between solutions and true one was generated in Fig. 7. As shown in Fig. 7, orbit accuracy is improved after adding these data, except for same-beam differential VLBI with 10 ps noise. The highest and most stable orbit determination accuracy can be reached by adding four-way data or three-way loop data.

These three methods, the same-beam differential VLBI, four-way Doppler, and three-way loop Doppler, are all effective for lander positioning. The four-way Doppler and three-way loop Doppler can play a part in improving orbital accuracy, but the same-beam differential VLBI data could not improve spacecraft orbit accuracy. A possible reason is that the same-beam differential VLBI data give information about the angles between the spacecraft and the lander, and cannot constrain the spacecraft orbit directly. The noise level of same-beam differential VLBI data directly affects the positioning accuracy of the lander, which could be increased by one order of magnitude for each order of magnitude improvement in same-beam differential VLBI data.

The four-way Doppler can improve orbital accuracy significantly as well as lander positioning. Our previous work showed that two-way data are more sensitive in the line-of-sight direction, while four-way data have a more rigorous geometric configuration (Li et al., 2016) due to the link line between the lander and the orbiter form an angle with the orbit plane. Therefore, the extra link in the four-way tracking mode between the lander and the orbiter could better constrain error in the tangential and normal directions and thus make complements the traditional two-way tracking mode (Ye, 2016).

The three-way loop Doppler and two-way Doppler shows high stability in the orbital accuracy as compared with the solution from two-way Doppler data alone. The improvement was similar to that from the four-way data. Furthermore, the three-way Doppler has the advantage that the orbital errors have less effect on the lander positioning than the four-way Doppler does and it is more intuitive and more convenient to implement in comparison to four-way Doppler model. Since the lander is stable on Mars, with massively increasing volume of tracking data, the three-way loop Doppler mode has the potential to solve orientation and rotation Parameters of Mars.

4. Conclusion

In this paper, we investigated three tracking modes that potentially could be employed during future Mars mission to constrain the positioning of the orbiter and lander. After adding the same-beam differential

Table 7

Initial orbit position difference between solution and true one using four-way and two-way data (estimated bias values, with the Landers position error of 1 km deviation and gravity field model error with a factor of three of the gravity field coefficient uncertainty).

Arc No.	Two-way Doppler only				Two-way Doppler and four-way Doppler				
	Δx (m)	Δy (m)	Δz (m)	Errors(m)	Δx (m)	Δy (m)	Δz (m)	Errors(m)	Bias (mm/s)
1	2.342	-3.450	-1.861	4.566	2.489	-3.669	-1.978	4.854	2.000
2	0.268	-0.115	-0.761	0.815	0.531	-0.251	-1.584	1.689	2.000
3	0.313	0.741	-3.030	3.135	0.137	0.281	-1.115	1.157	2.000
4	0.106	-0.186	0.380	0.436	0.133	-0.351	0.663	0.761	2.000
5	1.551	1.371	-2.689	3.393	0.413	-0.344	-0.661	0.851	2.000
6	1.789	0.176	-7.484	7.697	0.784	0.077	-3.286	3.379	2.000
7	-0.081	0.172	-0.076	0.204	-0.130	0.269	-0.129	0.325	2.000

Table 8

The iterative process of the lander for four-way Doppler data.

Number of iterations	without the gravity field model errors and measurement bias			with the gravity field model errors and measurement bias		
	Δx (m)	Δy (m)	Δz (m)	Δx (m)	Δy (m)	Δz (m)
1	-866.989	-862.227	863.430	-868.606	-867.197	867.299
2	-122.648	-118.451	120.158	-120.491	-119.361	119.883
3	-10.785	-10.954	10.734	-10.712	-11.385	11.483
4	0.215	-0.194	0.387	-0.183	-1.625	1.408
Total	-1000.207	-999.826	999.709	-999.992	-999.568	1000.073
Errors	0.207	-0.174	0.291	-0.008	-0.432	-0.073
3σ	± 0.467	± 0.696	± 0.527	± 0.467	± 0.696	± 0.527

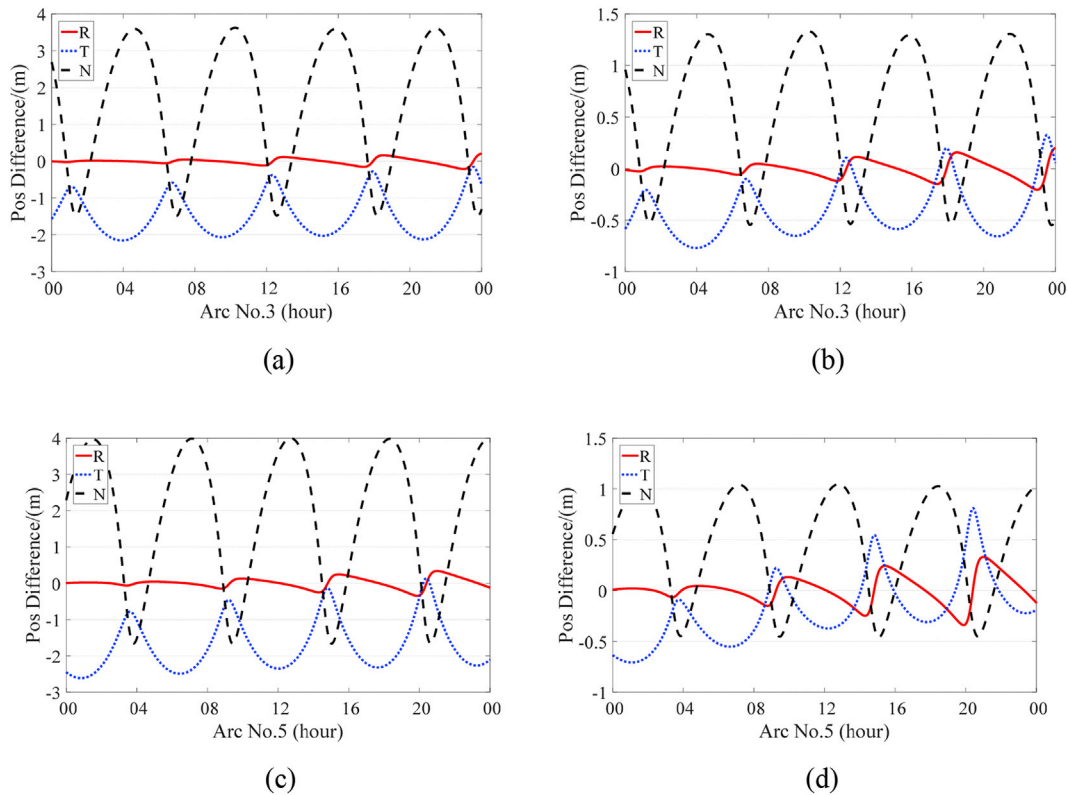


Fig. 6. The Differences between true orbit and reconstructed orbits from two-way Doppler and four-way Doppler. (The figure (a) shows orbit position differences of arc No. 3 using two-way Doppler, and the figure (b) shows this differences after including four-way Doppler. The figure (c) shows orbit position differences of arc No. 5 using two-way Doppler, and the figure (d) shows these differences after including four-way Doppler).

VLBI observations, the orbit accuracy cannot be greatly improved because VLBI data are only sensitive to the angular difference between two objects. Nevertheless, the position of the orbiter could be restrained in some arcs, and the lander position accuracy could reach around 60 m

with same-beam differential VLBI noise of 10 ps. After combining the four-way orbiter-lander data, the accuracy of the orbit was improved doubly when compared to one derived from the two-way Doppler, and the positional accuracy of the lander reaches the decimeter level. By

Table 9

Initial orbit position difference between solution and true one using three-way loop and two-way data (estimated bias values, with the Landers position error of 1 km deviation and gravity field model errors with a factor of three of the gravity field coefficient uncertainty).

Arc No.	Two-way Doppler only				Two-way Doppler and three-way loop Doppler				
	Δx (m)	Δy (m)	Δz (m)	Errors(m)	Δx (m)	Δy (m)	Δz (m)	Errors(m)	Bias (mm/s)
1	2.342	-3.450	-1.861	4.566	2.401	-3.539	-1.908	4.682	2.000
2	0.268	-0.115	-0.761	0.815	0.474	-0.222	-1.405	1.499	2.000
3	0.313	0.741	-3.030	3.135	0.155	0.327	-1.311	1.360	2.000
4	0.106	-0.186	0.380	0.436	0.129	-0.326	0.620	0.712	2.000
5	1.551	1.371	-2.689	3.393	0.443	-0.371	-0.715	0.919	2.000
6	1.789	0.176	-7.484	7.697	1.609	0.159	-6.731	6.922	2.000
7	-0.081	0.172	-0.076	0.204	-0.125	0.259	-0.124	0.313	2.000

Table 10

The iterative process of the lander for three-way loop data.

Number of iterations	without the gravity field model errors and measurement bias			adding gravity field model errors and measurement bias		
	Δx (m)	Δy (m)	Δz (m)	Δx (m)	Δy (m)	Δz (m)
1	-886.827	-887.513	887.320	-884.534	-884.478	885.170
2	-101.075	-99.832	-99.193	-102.287	-101.788	100.893
3	-11.254	-10.767	11.462	-12.069	-11.305	12.017
4	-1.073	-1.485	1.459	-1.126	-1.762	1.690
Total	-1000.229	-999.597	999.434	-1000.016	-999.333	999.770
Errors	0.229	-0.403	0.566	0.016	-0.667	0.230
3σ	± 0.567	± 0.893	± 0.845	± 1.127	± 0.891	± 0.844

Table 11

The influence of orbital errors on lander positioning.

Errors	Four-way Doppler	Three-way loop Doppler
X (m)	13.458	-0.817
Y (m)	17.337	-20.712
Z (m)	-52.418	-8.727
Total (m)	56.828	22.491

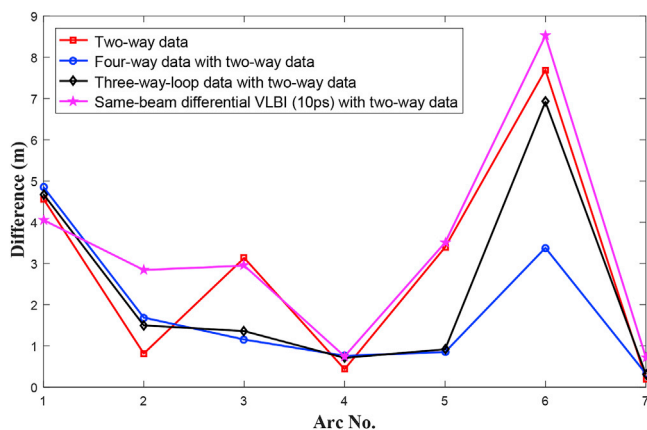


Fig. 7. Initial orbit position difference between solutions and true one (gravity field model errors and measurement bias are not considered). The difference is the total discrepancy from initial orbit position in J2000 frame.

considering the three-way loop Doppler data, the accuracy of orbit and lander position is consistent with those from the four-way orbiter-lander Doppler.

The simulation results show that our proposed tracking models for the orbiter-lander have advantages when locating the position of the lander, and improve the accuracy of orbit determination. This work could provide a reference for the future Mars mission. In the future, the further contribution of these tracking modes towards Mars orientation parameters solution and gravity field modeling will be investigated.

Acknowledgments

We appreciate Prof. Liu Qinghui from Shanghai Astronomical Observatory for his insightful discussion. We are grateful to NASA and ESA for providing models and data to make this research possible. The Martian topography map source data is from Mars orbiter laser altimeter (MOLA) science team. This research was funded by National Scientific Foundation of China (Grant No. 41374024, 41174019), Innovation Group of Natural Fund of Hubei Province (Grant No. 2015CFA011), and the CAS Key Laboratory of Planetary Sciences, Shanghai Astronomical Observatory, Chinese Academy of Sciences. Open Research Fund of Key Laboratory of Space Object Measurement and the Opening Project of Shanghai Key Laboratory of Space Navigation and Positioning Techniques (No. KFKT_201703) also support this work. The numerical calculations in this paper have been done on the supercomputing system in the Supercomputing Center of Wuhan University.

References

Border, J.S., Folkner, W.M., Kahn, R.D., et al., 1991. Precise tracking of the Magellan and Pioneer Venus orbiters by same-beam interferometry. *Adv. Astronaut. Sci.* 75 (2), 1269–1288.

Chen, M., Liu, Q.H., 2010. Study on differential phase delay closure of same-beam differential VLBI. In: *Computer Engineering and Technology (ICCET), 2010 2nd International Conference on* (Vol. 5, pp. V5-88). IEEE.

Counselman, C.C., Hinteregger, H.F., Shapiro, I.I., 1972. Astronomical applications of differential interferometry. *Science* 178 (4061), 607–608.

Dong, G., Xu, D., Li, H., Zhou, H., 2016. Initial result of the Chinese deep space stations' coordinates from Chinese domestic vlbi experiments. *Sci. China Inf. Sci.* 60 (1), 012203.

Edwards Jr., C.D., Kahn, R.D., Folkner, W.M., et al., 1991. Differential tracking data types for accurate and efficient Mars planetary navigation. *Proc. Inst. Navig. Annu. Meet.* 47, 39–46.

Goossens, S., Matsumoto, K., Ishihara, Y., Liu, Q., Kikuchi, F., Noda, H., 2009. Results for orbit determination of the three satellites of Kaguya. *J. Geol. Soc. Jpn.* 55, 255–268.

Goossens, S., Matsumoto, K., Liu, Q., Kikuchi, F., Sato, K., Hanada, H., Iwata, T., 2011. Lunar gravity field determination using SELENE same-beam differential VLBI tracking data. *J. Geodes.* 85 (4), 205–228.

Hanada, H., et al., 2008. VLBI for better gravimetry in SELENE. *Adv. Space Res.* 42, 341–346. <https://doi.org/10.1016/j.asr.2007.11.003>.

Huang, C., Ries, J.C., Tapley, B.D., Watkins, M.M., 1990. Relativistic effects for near-earth satellite orbit determination. *Celestial Mech. Dyn. Astron.* 48 (2), 167–185.

Jin, S.G., Zhang, T.Y., 2014. Automatic detection of impact craters on Mars using a modified adaboosting method. *Planet. Space Sci.* 99, 112–117. <https://doi.org/10.1016/j.pss.2014.04.021>.

- Jin, S.G., Wang, J., Zhang, H., Zhu, W.Y., 2004. Real-time monitoring and prediction of the total ionospheric electron content by means of GPS observations. *Chin. Astron. Astrophys.* 28 (3), 331–337. <https://doi.org/10.1016/j.chinastron.2004.07.008>.
- Jin, S.G., Arivazhagan, S., Araki, H., 2013. New results and questions of lunar exploration from SELENE, Chang'E-1, Chandrayaan-1 and LRO/LCROSS. *Adv. Space Res.* 52 (2), 285–305. <https://doi.org/10.1016/j.asr.2012.11.022>.
- Jin, S.G., Jin, R., Li, D., 2016. Assessment of BeiDou differential code bias variations from multi-GNSS network observations. *Ann. Geophys.* 34 (2), 259–269. <https://doi.org/10.5194/angeo-34-259-2016>.
- Kahn, R.D., Folkner, W.M., Edwards, C.D., et al., 1992. Position determination of spacecraft at Mars using earth-based differential tracking. *Adv. Astronaut. Sci.* 76 (2), 1545–1562.
- King, R.W., Counselman III, C.C., Shapiro, I.I., 1976. Lunar dynamics and selenodesy: results from analysis of VLBI and laser data. *J. Geophys. Res.* 81 (35), 6251–6256.
- Konopliv, A.S., Park, R.S., Folkner, W.M., 2016. An improved JPL Mars gravity field and orientation from Mars orbiter and lander tracking data. *Icarus* 274, 253–260.
- Li, F., Ye, M., Yan, J., Hao, W., Barriot, J.P., 2016. A simulation of the Four-way lunar Lander–Orbiter tracking mode for the Chang'E-5 mission. *Adv. Space Res.* 57 (11), 2376–2384.
- Liu, Q.H., Kikuchi, F., Matsumoto, K., Goossens, S., Hanada, H., Harada, Y., Asari, K., 2010. Same-beam VLBI observations of SELENE for improving lunar gravity field model. *Radio Sci.* 45 (2).
- Liu, Q.H., Wu, Y.J., Huang, Y., et al., 2015. Mars rover positioning technology based on Same-beam differential VLBI (in Chinese). *Sci. Sin. Phys. Mech. Astron.* 45, 099502 <https://doi.org/10.1360/SSPMA2015-00287>.
- Liu, J.D., Wei, E., Jin, S.G., 2017. Cruise orbit determination of Mars from combined optical celestial techniques and X-ray pulsars. *J. Navig.* 70 (4), 719–734. <https://doi.org/10.1017/S0373463316000874>.
- Liu, J.D., Wei, E., Jin, S.G., Liu, J., 2018. Absolute navigation and positioning of Mars rover using gravity-aided dead-reckoned odometry. *J. Navig.* <https://doi.org/10.1017/S0373463317000893>.
- Ye, Mao, 2016. Development of lunar spacecraft precision orbit determination software system and research on a four-way relay tracking measurement mode. *Acta Geod. Cartogr. Sinica* 45 (9), 1132–1132.
- Matsumoto, K., Hanada, H., Namiki, N., Iwata, T., Goossens, S., Tsuruta, S., Kawano, N., Rowlands, D., 2008. A simulation study for anticipated accuracy of lunar gravity field model by SELENE tracking data. *Adv. Space Res.* 42, 331–336. <https://doi.org/10.1016/j.asr.2007.03.066>.
- Montenbruck, Eberhard, O., 2012. *Satellite Orbits: Models, Methods, Applications*. Springer Verlag.
- Moyer, Theodore D., 2005. *Formulation for Observed and Computed Values of Deep Space Network Data Types for Navigation*, vol. 3. John Wiley & Sons.
- Namiki, N., Hanada, H., Tsubokawa, T., et al., 1999. Selenodetic experiments of SELENE: relay subsatellite, differential VLBI, and laser altimeter. *Adv. Space Res.* 23, 1817–1820.
- Namiki, N., Iwata, T., Matsumoto, K., Hanada, H., Noda, H., Goossens, S., Ishihara, Y., 2009. Farside gravity field of the Moon from four-way Doppler measurements of SELENE (Kaguya). *Science* 323 (5916), 900–905.
- Nandi, S., Border, J.S., Folkner, W.M., 1993. Demonstration of use of a real time tone tracker to obtain same beam interferometry data. *Adv. Astronaut. Sci.* 82 (2), 1061–1070.
- Preston, R.A., Hildebrand, C.E., Purcell, G.H., et al., 1986. Determination of venus winds by ground-based radio tracking of the VEGA balloons. *Science* 231, 1414–1416.
- Shapiro, I.I., 1964. Fourth test of general relativity. *Phys. Rev. Lett.* 13 (26), 789.
- Smith, J.R., Ramos, R., 1980. Data acquisition for measuring the wind on venus from pioneer venus. *IEEE Trans. Geosci. Rem. Sens.* GE 18 (1), 126–130.
- Smith, D.E., Zuber, M.T., Frey, H.V., et al., 2001a. Mars orbiter laser altimeter: experiment summary after the first year of global mapping of mars. *J. Geophys. Res.* 106, 23689–23722. <https://doi.org/10.1029/2000JE001364>.
- Smith, D.E., Zuber, M.T., Frey, H.V., Garvin, J.B., Head, J.W., Muhleman, D.O., Banerdt, W.B., 2001b. Mars orbiter laser altimeter: experiment summary after the first year of global mapping of mars. *J. Geogr. Reg. Planet.* 106 (E10), 23689–23722.
- Stewart, A.I.F., 1987. Revised Time Dependent Model of the Martian Atmosphere for Use in Orbit Lifetime and Sustainance Studies. Technical Report, JPL PO NQ-802429. University of Colorado, Boulder, Co.
- Tapley, B., Schutz, B., Born, G.H., 2004. *Statistical Orbit Determination*. Academic Press, Boston, MA.
- Tenzer, R., Eshagh, M., Jin, S.G., 2015a. Martian sub-crustal stress from gravity and topographic models. *Earth Planet Sci. Lett.* 425, 84–92. <https://doi.org/10.1016/j.epsl.2015.05.049>.
- Tenzer, R., Chen, W., Tsoulis, D., et al., 2015b. Analysis of the refined CRUST1.0 crustal model and its gravity field. *Surv. Geophys.* 36 (1), 139–165. <https://doi.org/10.1007/s10712-014-9299-6>.
- Thornton, C.L., Border, J.S., 2000. Radiometric tracking techniques for deep-space navigation. Monograph 1, Deep-space Communications and Navigation Series. Jet Propulsion Laboratory, JPL Publication, pp. 00–11.
- Tommei, G., Milani, A., Vokrouhlický, D., 2010. Light-time computations for the BepiColombo radio science experiment. *Celestial Mech. Dyn. Astron.* 107 (1–2), 285–298.
- Wei, E., Jin, S.G., Zhang, Q., Liu, J., Li, X., Yan, W., 2013. Autonomous navigation of Mars probe using X-ray pulsars: modeling and results. *Adv. Space Res.* 51 (5), 849–857. <https://doi.org/10.1016/j.asr.2012.10.009>.
- Wei, E., Li, X., Jin, S.G., Liu, J., 2016. Effect of lunar gravity models on Chang'E-2 orbit determination using VLBI tracking data. *Gedrag Gezond.* 7 (6), 406–415. <https://doi.org/10.1016/j.geog.2016.09.001>.
- Williams, J.G., Boggs, D.H., Folkner, W.M., 2008. DE421 lunar Orbit, Physical Librations, and Surface Coordinates. JPL IOM 335-JW, DB. WF-20080314–001, March 14.
- Yan, J.G., Goossens, S., Matsumoto, K., et al., 2012. CEGM02: an improved lunar gravity model using Chang'E-1 orbital tracking data. *Planet. Space Sci.* 62, 1–9.
- Yan, J., Yang, X., Ye, M., Li, F., Jin, W., Barriot, J.P., 2017. Independent mars spacecraft precise orbit determination software development and its applications. *Astrophys. Space Sci.* 362 (7), 123.